Journal of Computational and Applied Mathematics 394 (2021) 113532

Contents lists available at ScienceDirect

Journal of Computational and Applied Mathematics

journal homepage: www.elsevier.com/locate/cam

Generalized SAV approaches for gradient systems

Qing Cheng [a,*], Chun Liu [a,1], Jie Shen [b,2]

[a] Department of Applied Mathematics, Illinois Institute of Technology, Chicago, IL 60616, USA
[b] Department of Mathematics, Purdue University, West Lafayette, IN 47907, USA

ARTICLE INFO

Article history:
Received 5 July 2020
Received in revised form 8 February 2021

Keywords:
Gradient system
SAV approach
Energy stability
Phase-field

ABSTRACT

We propose in this paper three generalized auxiliary scalar variable (G-SAV) approaches for developing, efficient energy stable numerical schemes for gradient systems. The first two G-SAV approaches allow a range of functions in the definition of the SAV variable, furthermore, the second G-SAV approach only requires the total free energy to be bounded from below as opposed to the requirement that the nonlinear part of the free energy to be bounded from below. On the other hand, the third G-SAV approach is unconditionally energy stable with respect to the original free energy as opposed to a modified energy. Ample numerical results for various gradient systems are presented to validate the effectiveness and accuracy of the proposed G-SAV approaches.

Published by Elsevier B.V.

1. Introduction

Many science and engineering problems can be modeled by gradient systems, and tremendous efforts have been devoted to their numerical approximations. We refer the readers to a recent review paper on this topic [1]. Recently, a new class of method, the so called SAV method was introduced in (cf. [2,3]). The method is inspired by the IEQ method [4], it inherits all advantages of the IEQ method but it possesses a key additional advantage that the SAV schemes lead to decoupled linear systems with constant coefficients at each time step.

The SAV approach has received much attention since its introduction due to its efficiency, flexibility and accuracy. It has been applied to various situations, and numerous modifications/extensions have been proposed, including the multiple SAV approach [5], the Runge–Kutta SAV (RK-SAV) method [6] in which it is shown that the SAV approach coupled with diagonally implicit high-order Runge–Kutta method is unconditionally energy stable, stabilized SAV (S-SAV) approach [7] where different stabilization terms are added to deal with highly stiff nonlinear potentials, generalized positive auxiliary variable (gPAV) method [8] which can deal with general dissipative systems, and the Lagrange multiplier approach [9] which can dissipate/conserve the original energy instead of a modified energy in the SAV approaches, to just name a few.

The key for preserving energy dissipation in IEQ and SAV approaches is to introduce auxiliary variables so that nonlinear terms can be treated explicitly while being unconditionally energy stable. In the original IEQ and SAV approaches, the new SAV variable is chosen to the square root of nonlinear part of the energy density or energy functional, which, on the one hand, leading to unconditional energy stability and linear decoupled schemes, but on the other hand, requiring the nonlinear part of the free energy to be bounded from below so its application is somewhat limited [10,11].

* Corresponding author.
E-mail addresses: qcheng4@iit.edu (Q. Cheng), cliu124@iit.edu (C. Liu), shen7@purdue.edu (J. Shen).

[1] The work of Chun Liu and Qing Cheng is partially supported by NSF (National Science Foundation), USA Grant DMS-1759535 and United Stated-Israel Binational Science Foundation (BSF) Grant 2024246.

[2] The work of Jie Shen is partially supported by NSF (National Science Foundation), USA Grant DMS-2012585 and AFOSR (Air Force Office of Scientific Research), USA Grant FA9550-20-1-0309.

https://doi.org/10.1016/j.cam.2021.113532
0377-0427/Published by Elsevier B.V.

The goal of this paper is to propose three generalized SAV (G-SAV) approaches which, respectively, allow a range of choices for the function in the definition of the SAV, extend the applicability of the original SAV approach, and lead to unconditionally energy stable schemes with respect to the original energy, while keeping other essential advantages of the original SAV approach. A small price to pay for these advantages is that the G-SAV approach requires solving a nonlinear algebraic equation for the SAV variable with negligible computational cost.

The remainder of this paper is structured as follows. In Section 2, we present the three G-SAV approaches for gradient systems. In Section 3, we extend the G-SAV approach to for gradient systems with multiple nonlinear potentials and/or multiple components. In Section 4, we present several numerical simulations by using the new approaches and compare with existing schemes. Some concluding remarks are given in the last section.

2. The G-SAV approaches

We present in this section the G-SAV approaches for developing energy stable numerical schemes for gradient systems. To simplify the presentation, we consider first gradient systems with a single component, extension to gradient systems with multi-components models will be presented later in this section.

Following [3], we consider a system with total free energy in the form

$$E(\phi) = \int_\Omega \frac{1}{2}\mathcal{L}\phi\cdot\phi + F(\phi)d\boldsymbol{x}, \tag{2.1}$$

where $\mathcal{L}$ is certain linear positive operator, $F(\phi)$ is a nonlinear potential functional. Then a general gradient system with the above free energy is

$$\phi_t = -\mathcal{G}\frac{\delta E(\phi)}{\delta\phi},$$

which, for the sake of numerical approximation, we rewrite by introducing $\mu = \frac{\delta E(\phi)}{\delta\phi}$ as

$$\begin{aligned} &\phi_t = -\mathcal{G}\mu,\\ &\mu = \mathcal{L}\phi + F'(\phi). \end{aligned} \tag{2.2}$$

where $\mathcal{G}$ is a positive or skew symmetric operator describing the relaxation process of the system. To fix the idea, we assume that the boundary conditions are either periodic or such that it allows for integration by parts without introducing additional boundary terms, e.g., if $\mathcal{G} = -\Delta$, the boundary conditions should be

$$\partial_{\mathbf{n}}\phi|_{\partial\Omega} = \partial_{\mathbf{n}}\mu|_{\partial\Omega} = 0, \tag{2.3}$$

where $\mathbf{n}$ is the unit outward normal on the boundary $\partial\Omega$.

Taking the inner products of the first two equations with μ and $-\phi_t$ respectively, integrating by part and summing up the results, we obtain the following energy dissipation law:

$$\frac{d}{dt}E(\phi) = -(\mathcal{G}\mu,\mu), \tag{2.4}$$

where, and in the sequel, $(\cdot,\cdot)$ denotes the inner product in $L^2(\Omega)$ with the L^2-norm denoted by $\|\cdot\|$.

2.1. The first G-SAV approach

We consider here the generalization of the original SAV approach [3,12]. We assume $\int_\Omega F(\phi)d\boldsymbol{x} > -C_0 + 1$. For a given invertible function $G : [-C_0, \infty) \to [a, \infty)$ with $a > 0$, we rewrite the original energy (2.1) as

$$E(\phi) = \int_\Omega \frac{1}{2}\mathcal{L}\phi\cdot\phi d\boldsymbol{x} + G^{-1}\{G(\int_\Omega F(\phi)d\boldsymbol{x} + C_0)\}. \tag{2.5}$$

We define a SAV $r(t) := G(\int_\Omega F(\phi)d\boldsymbol{x} + C_0)$ and derive from $G^{-1}(r) = \int_\Omega F(\phi)d\boldsymbol{x} + C_0$ that

$$\frac{d}{dt}G^{-1}(r) = (F'(\phi),\phi_t). \tag{2.6}$$

Hence, we can rewrite system (2.2) into the following equivalent form

$$\partial_t\phi = -\mathcal{G}\mu, \tag{2.7}$$

$$\mu = \mathcal{L}\phi + \frac{r}{G(\int_\Omega F(\phi)d\boldsymbol{x} + C_0)}F'(\phi), \tag{2.8}$$

$$\frac{d}{dt}G^{-1}(r) = \frac{r}{G(\int_\Omega F(\phi)d\boldsymbol{x} + C_0)}(F'(\phi),\phi_t), \tag{2.9}$$

with $r(0) := G(\int_\Omega F(\phi(\cdot,0))d\boldsymbol{x} + C_0)$.

Taking the inner products of the first two equations with μ and $-\phi_t$ respectively, summing up the results along with the third equation, we obtain the following energy dissipation law:

$$\frac{d}{dt}\tilde{E}(\phi) = -(\mathcal{G}\mu, \mu), \tag{2.10}$$

where $\tilde{E}(\phi) = \int_\Omega \frac{1}{2}\mathcal{L}\phi\cdot\phi d\boldsymbol{x} + G^{-1}(r)$ which equals exactly $E(\phi)+C_0$.

As an example, we construct below a second-order Crank–Nicolson scheme for the system (2.7)–(2.9):

$$\frac{\phi^{n+1}-\phi^n}{\delta t} = -\mathcal{G}\mu^{n+1/2}, \tag{2.11}$$

$$\mu^{n+1/2} = \mathcal{L}\phi^{n+1/2} + \frac{r^{n+1/2}}{G(\int_\Omega F(\phi^{*,n+1/2})d\boldsymbol{x}+C_0)}F'(\phi^{*,n+1/2}), \tag{2.12}$$

$$\frac{(G^{-1}(r))^{n+1}-(G^{-1}(r))^n}{\delta t} = \frac{r^{n+1/2}}{G(\int_\Omega F(\phi^{\star,n+\frac{1}{2}})d\boldsymbol{x}+C_0)}(F'(\phi^{*,n+1/2}), \frac{\phi^{n+1}-\phi^n}{\delta t}), \tag{2.13}$$

where, for any sequence $\{g^k\}$, $g^{k+1/2} = \frac{1}{2}(g^{k+1}+g^k)$ and $g^{*,n+1/2} = \frac{3}{2}g^k - \frac{1}{2}g^{k-1}$.

Taking the inner products of (2.11) with $\mu^{n+1/2}$ and of (2.12) with $-\frac{\phi^{n+1}-\phi^n}{\delta t}$, summing up the results and taking into account (2.13), we immediate obtain the following: The scheme (2.11)–(2.13) satisfies unconditionally the following discrete energy conservation law:

$$\tilde{E}(\phi^{n+1}) - \tilde{E}(\phi^n) = -\Delta t(\mathcal{G}\mu^{n+1/2}, \mu^{n+1/2}),$$

where $\tilde{E}(\phi^k) = \int_\Omega \frac{1}{2}\mathcal{L}\phi^k\cdot\phi^k d\boldsymbol{x} + (G^{-1}(r))^k$ is a modified energy.

We note that in the time discrete case $\tilde{E}(\phi^k) \neq E(\phi^k)$ since $(G^{-1}(r))^k \neq \int_\Omega F(\phi^k)d\boldsymbol{x}$.

The scheme (2.11)–(2.13) is a weakly coupled nonlinear system but it can still be implemented efficiently as follows. Since $\phi^{n+\frac{1}{2}} = \frac{\phi^{n+1}+\phi^n}{2}$ and we rewrite (2.11) as

$$\frac{\phi^{n+\frac{1}{2}}-\phi^n}{\frac{1}{2}\delta t} = -\mathcal{G}\mu^{n+1/2}. \tag{2.14}$$

Setting $\xi^{n+1/2} = \frac{r^{n+1/2}}{G(\int_\Omega F(\phi^{*,n+1/2})+C_0 d\boldsymbol{x})}$ and writing

$$\phi^{n+1/2} = \phi_1^{n+1/2} + \xi^{n+1/2}\phi_2^{n+1/2},\ \ \mu^{n+1/2} = \mu_1^{n+1/2} + \xi^{n+1/2}\mu_2^{n+1/2}, \tag{2.15}$$

in (2.11)–(2.12), we find that $(\phi_i^{n+\frac{1}{2}}, \mu_i^{n+\frac{1}{2}})$ $(i=1,2)$ can be determined by solving the following decoupled linear systems with constant coefficients:

$$\frac{\phi_1^{n+\frac{1}{2}}-\phi^n}{\frac{1}{2}\delta t} = -\mathcal{G}\mu_1^{n+1/2}, \tag{2.16}$$

$$\mu_1^{n+1/2} = \mathcal{L}\phi_1^{n+1/2}, \tag{2.17}$$

and

$$\frac{\phi_2^{n+\frac{1}{2}}}{\frac{1}{2}\delta t} = -\mathcal{G}\mu_2^{n+1/2}, \tag{2.18}$$

$$\mu_2^{n+1/2} = \mathcal{L}\phi_2^{n+1/2} + F'(\phi^{*,n+1/2}). \tag{2.19}$$

Once $(\phi_1^{n+\frac{1}{2}}, \phi_2^{n+\frac{1}{2}})$ are known, we plug $\phi^{n+\frac{1}{2}} = \phi_1^{n+\frac{1}{2}} + \xi^{n+\frac{1}{2}}\phi_2^{n+\frac{1}{2}}$ and $r^{n+1/2} = \xi^{n+1/2}G(\int_\Omega F(\phi^{*,n+1/2})d\boldsymbol{x} + C_0)$ into Eq. (2.13) to obtain a nonlinear algebraic equation for $\xi^{n+\frac{1}{2}}$. This nonlinear algebraic equation can be solved by a Newton iteration with initial guess 1, since by definition $\xi^{n+\frac{1}{2}}$ is a second-order approximation for 1. Finally we can obtain (ϕ^{n+1}, μ^{n+1}) from (2.15). Note that the cost of solving the nonlinear algebraic equation is negligible, so the total cost of the new G-SAV scheme is essentially the same as the original SAV schemes.

We remark that we are unable to show that $\{(G^{-1}(r))^n\}$ have a lower bound, although numerical results presented in Section 4 indicate that, when the time step is not too large, $\{(G^{-1}(r))^n\}$ are well bounded from below and lead to very good numerical results for a range of G. Another drawback of the first G-SAV approach is that the nonlinear part of the free energy has to be bounded from below. Therefore, we propose in the following two other G-SAV approaches which overcome these shortcomings.

2.2. The second G-SAV approach

The first G-SAV approach requires $\int_\Omega F(\phi)dx$ to be bounded from below, and this may not be true for some gradient systems, such as the MBE model without slope selection [10], the binary phase field fluid–surfactant system [13] and the phase field nuclear architecture reorganization model [14]. Hence, we construct the second G-SAV approach which only requires that $E(\phi) > -C_0 + 1$ using a idea introduced in [15]. Furthermore, it ensures that $\{(G^{-1}(r))^n\}$ are bounded from below.

For a given invertible function $G : [-C_0, \infty) \to [a, \infty)$ with some constant $a > 0$, we define $r(t) = G(E(\phi) + C_0)$. Setting $\xi(t) = \frac{G^{-1}(r)}{E(\phi)+C_0} \equiv 1$, we can rewrite system (2.2) into the following equivalent form

$$\partial_t \phi = -\mathcal{G}\mu, \tag{2.20}$$

$$\mu = \mathcal{L}\phi + \xi F'(\phi), \tag{2.21}$$

$$\xi = \frac{G^{-1}(r)}{E(\phi) + C_0}, \tag{2.22}$$

$$\frac{d}{dt}G^{-1}(r) = -\xi(\mathcal{G}\mu, \mu), \tag{2.23}$$

with $r(0) := G(\int_\Omega E(\phi(\cdot, 0))d\boldsymbol{x})$.

Based on Eqs. (2.20)–(2.23), we can construct a second order BDF2 scheme as follows

$$\frac{3\phi^{n+1} - 4\phi^n + \phi^{n-1}}{2\delta t} = -\mathcal{G}\mu^{n+1}, \tag{2.24}$$

$$\mu^{n+1} = \mathcal{L}\phi^{n+1} + \eta^{n+1}F'(\phi^{n,\dagger}), \tag{2.25}$$

$$\xi^{n+1} = \frac{(G^{-1}(r))^{n+1}}{E(\phi^n) + C_0}, \ \eta^{n+1} = 1 - (1 - \xi^{n+1})^2, \tag{2.26}$$

$$\frac{(G^{-1}(r))^{n+1} - (G^{-1}(r))^n}{\delta t} = -\xi^{n+1}(\mathcal{G}\mu^{n+1}, \mu^{n+1}), \tag{2.27}$$

with $F'(\phi^{n,\dagger}) = F'(2\phi^n - \phi^{n-1})$. Note that in the above scheme, $(G^{-1}(r))^{n+1}$ is only a first-order approximation to $E(\phi(t_{n+1}))+C_0$. But since ξ^{n+1} is a first-order approximation to 1, we see that ϕ^{n+1}, μ^{n+1} are second-order approximation of $\phi(t_{n+1})$, $\mu(t_{n+1})$.

The above scheme can be efficiently implemented as follows. Writing

$$\phi^{n+1} = \phi_1^{n+1} + \eta^{n+1}\phi_2^{n+1}, \ \mu^{n+1} = \mu_1^{n+1} + \eta^{n+1}\mu_2^{n+1}, \tag{2.28}$$

in (2.24)–(2.25), we can determine $(\phi_i^{n+1}, \mu_i^{n+1})$ $(i = 1, 2)$ by solving the following decoupled systems:

$$\frac{3\phi_1^{n+1} - 4\phi^n + \phi^{n-1}}{2\delta t} = -\mathcal{G}\mu_1^{n+1}, \tag{2.29}$$

$$\mu_1^{n+1} = \mathcal{L}\phi_1^{n+1}, \tag{2.30}$$

and

$$\frac{3\phi_2^{n+1}}{2\delta t} = -\mathcal{G}\mu_2^{n+1}, \tag{2.31}$$

$$\mu_2^{n+1} = \mathcal{L}\phi_2^{n+1} + F'(\phi^{n,\dagger}). \tag{2.32}$$

It remains to determine ξ^{n+1}. To this end, we plug (2.28) and $(G^{-1}(r))^{n+1} = \xi^{n+1}E(\phi^n)$ into Eq. (2.27) to obtain a nonlinear algebraic system for ξ^{n+1} which can be solved with a Newton iteration at negligible cost.

As for the stability, we have the following result:

Theorem 2.1. *Given $(G^{-1}(r))^0 = E(\phi^0) + C_0 > 0$, we have $(G^{-1}(r))^{n+1} > 0$ and $\xi^{n+1} > 0$ for all $n \geq 0$, and the scheme (2.24)–(2.27) is unconditional energy stable in the sense that*

$$\frac{(G^{-1}(r))^{n+1} - (G^{-1}(r))^n}{\delta t} = -\xi^{n+1}(\mu^{n+1}, \mathcal{G}\mu^{n+1}). \tag{2.33}$$

Proof. Plugging equation (2.26) into Eq. (2.27), we obtain

$$(\frac{1}{\delta t} + \frac{(\mu^{n+1}, \mathcal{G}\mu^{n+1})}{E(\phi^n) + C_0})(G^{-1}(r))^{n+1} = \frac{(G^{-1}(r))^n}{\delta t}. \tag{2.34}$$

Therefore, if $(G^{-1}(r))^n > 0$, we derive from the above that $(G^{-1}(r))^{n+1} > 0$. From (2.26), we also have $\xi^{n+1} > 0$. □

We remark that we can also construct higher-order schemes based on this G-SAV approach similarly as in [15].

2.3. The third G-SAV approach

In the second G-SAV approach above, the energy stability is with a modified energy $G^{-1}(r)$. We can couple the second G-SAV approach with the Lagrange multiplier approach [9] to construct schemes which dissipate the original energy.

We still assume $E(\phi) > -C_0$, and rewrite system (2.2) into the following equivalent form

$$\partial_t \phi = -\mathcal{G}\mu, \tag{2.35}$$

$$\mu = \mathcal{L}\phi + \xi F'(\phi), \tag{2.36}$$

$$\xi(t) = \frac{E(\phi) + C_0}{E(\phi) + C_0}, \tag{2.37}$$

$$\frac{d}{dt}E(\phi) = -\xi(\mathcal{G}\mu, \mu), \tag{2.38}$$

with $\xi(t) \equiv 1$ in continue level. Then, a second order BDF2 scheme based on new system (2.35)–(2.38) is:

$$\frac{3\phi^{n+1} - 4\phi^n + \phi^{n-1}}{2\delta t} = -\mathcal{G}\mu^{n+1}, \tag{2.39}$$

$$\mu^{n+1} = \mathcal{L}\phi^{n+1} + \eta^{n+1}F'(\phi^{n,\dagger}), \tag{2.40}$$

$$\xi^{n+1} = \frac{E(\phi^{n+1}) + C_0}{E(\phi^n) + C_0}, \ \eta^{n+1} = 1 - (1 - \xi^{n+1})^2, \tag{2.41}$$

$$\frac{E(\phi^{n+1}) - E(\phi^n)}{\delta t} = -\xi^{n+1}(\mathcal{G}\mu^{n+1}, \mu^{n+1}). \tag{2.42}$$

The scheme (2.39)–(2.42) can also be solved efficiently as scheme the (2.24)–(2.27). Indeed, plugging (2.28) in (2.39)–(2.40), we can still determine $(\phi_i^{n+1}, \mu_i^{n+1})$ $(i = 1, 2)$ from (2.29)–(2.30) and (2.31)–(2.32). Finally, we plug (2.28) and $E(\phi^{n+1}) + C_0 = \xi^{n+1}(E(\phi^n) + C_0)$ into Eq. (2.42) to obtain a nonlinear algebraic system for ξ^{n+1} which can be solved with a Newton iteration at negligible cost.

Theorem 2.2. *Given $E(\phi^0) + C_0 > 0$, we have $E(\phi^{n+1}) + C_0 > 0$ and $\xi^{n+1} > 0$ for all $n \geq 0$, and the scheme (2.39)–(2.42) is unconditional energy stable in the sense that*

$$\frac{E(\phi^{n+1}) - E(\phi^n)}{\delta t} = -\xi^{n+1}(\mu^{n+1}, \mathcal{G}\mu^{n+1}). \tag{2.43}$$

Proof. We derive from (2.41) that

$$\left(\frac{1}{\delta t} + \frac{(\mu^{n+1}, \mathcal{G}\mu^{n+1})}{E(\phi^n) + C_0}\right)(E(\phi^{n+1}) + C_0) = \frac{E(\phi^n) + C_0}{\delta t}. \tag{2.44}$$

Obviously, if $E(\phi^n) + C_0 > 0$, we obtain $E(\phi^{n+1}) + C_0 > 0$, then $\xi^{n+1} > 0$. Hence, (2.42) indicates that the scheme is unconditionally energy stable. □

We emphasize that a distinct feature of the scheme (2.39)–(2.42) is that it is unconditionally energy stable with the original energy $E(\phi)$. Similarly, unconditionally stable higher-order version can be constructed as in [15].

2.4. Typical choices of the invertible function G

In principle one can choose any invertible function G in the first and second G-SAV approaches. We consider below some typical choices. Let the constant C_0 is chosen such that (i) in the first G-SAV approach, the nonlinear part of the free energy $\int_\Omega F(\phi)dx > -C_0$; or (ii) in the second G-SAV approach, the total free energy $E(\phi) > -C_0 + 1$.

Let $\alpha > 0$ be a given constant, we can choose $G(x) = (x + C_0)^\alpha : [-C_0 + 1, \infty) \to [1, \infty)$ with $G^{-1}(x) = x^{\frac{1}{\alpha}} - C_0$.

A special case is $\alpha = 1/2$. we show below that with a slight modification, this choice in the first G-SAV approach leads to the original SAV approach [12].

With $G(x) = \sqrt{x + C_0}$, we have $G^{-1}(x) = x^2 - C_0$, so Eq. (2.9) becomes

$$\frac{d}{dt}r^2 = 2rr_t = \frac{r}{G(\int_\Omega F(\phi)d\boldsymbol{x})}(F'(\phi), \phi_t), \tag{2.45}$$

and the scheme (2.11)–(2.13) becomes

$$\frac{\phi^{n+1} - \phi^n}{\delta t} = -\mathcal{G}\mu^{n+1/2}, \tag{2.46}$$

$$\mu^{n+1/2} = \mathcal{L}\phi^{n+1/2} + \frac{r^{n+1/2}}{\sqrt{\int_\Omega F(\phi^{*,n+1/2})d\boldsymbol{x} + C_0}} F'(\phi^{*,n+1/2}), \tag{2.47}$$

$$\frac{(r^2)^{n+1} - (r^2)^n}{\delta t} = \frac{r^{n+1/2}}{\sqrt{\int_\Omega F(\phi^{*,n+1/2})d\boldsymbol{x} + C_0}} (F'(\phi^{*,n+1/2}), \frac{\phi^{n+1} - \phi^n}{\delta t}). \tag{2.48}$$

Note that the above scheme is very similar but still different to the Crank–Nicolson scheme based on the original SAV approach. Here (2.48) is a quadratic equation for r^{n+1}, while it is a linear equation in the original SAV approach. However, if we divide r on both sides of (2.45), then discretize with a Crank–Nicolson scheme, we can replace (2.48) by

$$\frac{r^{n+1} - r^n}{\delta t} = \frac{1}{2\sqrt{\int_\Omega F(\phi^{*,n+1/2})d\boldsymbol{x} + C_0}} (F'(\phi^{*,n+1/2}), \frac{\phi^{n+1} - \phi^n}{\delta t}), \tag{2.49}$$

which, along with (2.46)–(2.47), is exactly the Crank–Nicolson scheme based on the original SAV approach. This is the only choice of G which would lead to a linear algebraic system for r^{n+1}!

Other suitable choices include:

- $G(x) = \exp(x + C_0) : [-C_0, \infty) \to [1, \infty)$ with $G^{-1}(x) = \ln x - C_0$;
- $G(x) = \ln(x + C_0) : [-C_0 + 1, \infty) \to [0, \infty)$ with $G^{-1}(x) = \exp(x) - C_0$.

2.5. An alternative G-SAV approach

As a comparison, we also consider an alternative G-SAV approach which essentially treats the SAV variable explicitly, thus it does not require solving a nonlinear algebraic equation for the SAV variable (see a special case in [16]). More precisely, we replace $r^{n+1/2}$ in (2.8)–(2.9) by its explicit extrapolation $r^{*,n+1/2}$, leading to the scheme

$$\frac{\phi^{n+1} - \phi^n}{\delta t} = -\mathcal{G}\mu^{n+1/2}, \tag{2.50}$$

$$\mu^{n+1/2} = \mathcal{L}\phi^{n+1/2} + \frac{r^{*,n+1/2}}{G(\int_\Omega F(\phi^{*,n+1/2})d\boldsymbol{x} + C_0)} F'(\phi^{*,n+1/2}), \tag{2.51}$$

$$\frac{(G^{-1}(r))^{n+1} - (G^{-1}(r))^n}{\delta t} = \frac{r^{*,n+1/2}}{G(\int_\Omega F(\phi^n)d\boldsymbol{x} + C_0)} (F'(\phi^{*,n+1/2}), \frac{\phi^{n+1} - \phi^n}{\delta t}). \tag{2.52}$$

Taking the inner products of (2.50) with μ^{n+1} and of (2.51) with $-\frac{\phi^{n+1}-\phi^n}{\delta t}$, summing up the results and taking into account (2.52), we have the following discrete energy law:

$$\tilde{E}(\phi^{n+1}) - \tilde{E}(\phi^n) = -\Delta t(\mathcal{G}\mu^{n+1/2}, \mu^{n+1/2}),$$

where $\tilde{E}(\phi^k) = \int_\Omega \frac{1}{2}\mathcal{L}\phi^k \cdot \phi^k d\boldsymbol{x} + (G^{-1}(r))^k$.

Since r^{n+1} is not present in (2.50)–(2.51), we can first determine (ϕ^{n+1}, μ^{n+1}) from (2.50)–(2.51) which is essentially a semi-implicit scheme. Once (ϕ^{n+1}, μ^{n+1}) is known, we can determine r^{n+1} from (2.52) which is a nonlinear algebraic equation. Hence, this approach is very simple to implement while being unconditionally energy stable with a modified energy. However, as we shall demonstrate with numerical experiments in Section 4, there is no essential improvement over the usual semi-implicit scheme if accuracy is also taken into account.

2.6. Some practical strategies

We discuss below two useful practices, stabilization and adaptive time stepping, which might dramatically improve the performance of SAV type schemes.

2.6.1. Stabilization

For problems with stiff nonlinear terms, one may have to use very small time steps to obtain accurate results with G-SAV approaches above. However, adding some proper stabilization terms may alleviate the time step constraints. To this end, instead of solving (2.2), we consider a perturbed system with two additional stabilization terms

$$\begin{aligned} &\phi_t = -\mathcal{G}\mu, \\ &\mu = \mathcal{L}\phi + \epsilon_1\phi_{tt} + \epsilon_2\mathcal{L}\phi_{tt} + F'(\phi), \end{aligned} \tag{2.53}$$

where $\epsilon_i,\ i=1,2$ are two small stabilization constants whose choices will depend on how stiff are the nonlinear terms. It is easy to see that the above system is a gradient flow with a perturbed free energy $E_\epsilon(\phi)=E(\phi)+\frac{\epsilon_1}{2}(\phi_t,\phi_t)+\frac{\epsilon_2}{2}(\mathcal{L}\phi_t,\phi_t)$ and satisfies the following energy law:

$$\frac{d}{dt}E_\epsilon(\phi)=-(\mathcal{G}\mu,\mu). \tag{2.54}$$

The schemes presented above for (2.2) can all be easily extended for (2.53) while keeping the same simplicity. For example, a second order scheme based on the first G-SAV approach is:

$$\frac{\phi^{n+1}-\phi^n}{\delta t}=-\mathcal{G}\mu^{n+1/2}, \tag{2.55}$$

$$\mu^{n+1/2}=\mathcal{L}\phi^{n+1/2}+\frac{\epsilon_1}{(\delta t)^2}(\phi^{n+1}-2\phi^n+\phi^{n-1}) + \frac{\epsilon_2}{(\delta t)^2}\mathcal{L}(\phi^{n+1}-2\phi^n+\phi^{n-1})+\frac{r^{n+\frac{1}{2}}}{G(\int_\Omega F(\phi^{\star,n})d\boldsymbol{x}+C_0)}F'(\phi^{\star,n}), \tag{2.56}$$

$$\frac{G^{-1}(r^{n+1})-G^{-1}(r^n)}{\delta t}=\frac{r^{n+\frac{1}{2}}}{G(\int_\Omega F(\phi^{\star,n})d\boldsymbol{x}+C_0)}(F'(\phi^{\star,n}),\frac{\phi^{n+1}-\phi^n}{\delta t}), \tag{2.57}$$

where $f^{n+1/2}=\frac{1}{2}(f^{n+1}+f^n)$ and $f^{*,n}=\frac{1}{2}(3f^n-f^{n-1})$ for any sequence $\{f^n\}$.

Taking the inner products of (2.55) with $\mu^{n+1/2}$ and of (2.56) with $-\frac{\phi^{n+1}-\phi^n}{\delta t}$, and summing up the results with (2.57), we obtain, after dropping some unnecessary terms and using the equality

$$(a-2b+c,a-b)=\frac{1}{2}\{(a-b)^2-(b-c)^2+(a-2b+c)^2\} \tag{2.58}$$

that the scheme (2.55)–(2.57) satisfies unconditionally the following discrete energy law:

$$E_\epsilon^{n+1}-E_\epsilon^n\le-\delta t(\mathcal{G}\mu^{n+1/2},\mu^{n+1/2}),$$

where $E_\epsilon^k=\int_\Omega\frac{1}{2}\mathcal{L}\phi^k\cdot\phi^k d\boldsymbol{x}+(G^{-1}(r))^k+\frac{\epsilon_1}{2}(\frac{\phi^k-\phi^{k-1}}{\delta t},\frac{\phi^k-\phi^{k-1}}{\delta t})+\frac{\epsilon_2}{2}(\mathcal{L}\frac{\phi^k-\phi^{k-1}}{\delta t},\frac{\phi^k-\phi^{k-1}}{\delta t})$.

It is clear that the above scheme can be efficiently implemented as the scheme (2.11)–(2.13).

2.6.2. Adaptive time stepping

To further improve the efficiency of G-SAV approaches, one can combine them with an adaptive time stepping method as demonstrated for the original SAV approaches in [5,9,12]. Similarly, we can also apply an adaptive time stepping strategy for G-SAV approaches since these schemes satisfy unconditionally a discrete energy dissipation law, so we can choose time step based on the accuracy only. Furthermore, the SAV variable in the G-SAV approaches provides a natural criteria for selecting time step size. For example, in the first G-SAV approach, we can use $|\frac{r^{n+1}}{G(\int_\Omega F(\phi^{k+1})d\boldsymbol{x}+C_0)}-1|$ as an additional indicator.

3. Extensions

For the sake of simplicity, we presented the G-SAV approaches using the gradient system with a single component and a single nonlinear potential as an example. The G-SAV approaches can be easily extended to gradient system with multiple components and/or multiple nonlinear potentials.

To simplify our presentation, we shall only consider the first G-SAV approach and assume, without loss of generality, $\int_\Omega F(\phi_1,\phi_2,\dots,\phi_m)d\boldsymbol{x}>1$ or $\int_\Omega F_i(\phi_1,\phi_2,\dots,\phi_m)d\boldsymbol{x}>1$ for any i. The extensions to the other two G-SAV approaches can be constructed similarly.

3.1. Extension to gradient systems with multiple nonlinear potentials

While the G-SAV approaches can be directly applied to gradient systems with multiple nonlinear potentials, e.g., $F(\phi)=\sum_{i=1}^m F_i(\phi)d\boldsymbol{x}$, it may require exceedingly small time steps to achieve desired accuracy if properties of the multiple nonlinear terms are with very different stiffness. It is shown in [5] that better efficiency and accuracy can be achieved by introducing multiple SAVs, leading to the so called MSAV approach. We extend below the MSAV approach for such situations.

Consider the free energy

$$E(\phi)=\int_\Omega\frac{1}{2}\mathcal{L}\phi\cdot\phi+\sum_{i=1}^m F_i(\phi)d\boldsymbol{x}, \tag{3.1}$$

then using multiple SAVs may achieve better accuracy for numerical simulation which has been observed in [5]. The gradient flow with multiple nonlinear potentials is formulated as the following form

$$\begin{aligned}&\phi_t = -\mathcal{G}\mu,\\ &\mu = \mathcal{L}\phi + \sum_{i=1}^{m} F_i'(\phi),\end{aligned} \tag{3.2}$$

with suitable boundary conditions. Following the G-SAV approach, we rewrite the energy (3.1) as

$$E(\phi) = \int_\Omega \frac{1}{2}\mathcal{L}\phi\cdot\phi d\boldsymbol{x} + \sum_{i=1}^{m} G_i^{-1}\{G_i(\int_\Omega F_i(\phi)d\boldsymbol{x})\}, \tag{3.3}$$

where G_i $(i = 1, 2, \ldots, m)$ are certain invertible functions. Introducing m new SAV variables

$$r_i = G_i(\int_\Omega F_i(\phi)d\boldsymbol{x}), \quad i = 1, 2, \ldots, m, \tag{3.4}$$

we can rewrite (3.2) in the following equivalent form

$$\partial_t\phi = -\mathcal{G}\mu, \tag{3.5}$$

$$\mu = \mathcal{L}\phi + \sum_{i=1}^{m} \frac{r_i}{G_i(\int_\Omega F_i(\phi)d\boldsymbol{x})}F_i'(\phi), \tag{3.6}$$

$$\frac{d}{dt}G_i^{-1}(r_i) = \frac{r_i}{G_i(\int_\Omega F_i(\phi)d\boldsymbol{x})}(F_i'(\phi), \phi_t), \quad i = 1, 2, \ldots, m. \tag{3.7}$$

Then a second-order Crank–Nicolson scheme can be constructed for the system (3.5)–(3.7)

$$\frac{\phi^{n+1}-\phi^n}{\delta t} = -\mathcal{G}\mu^{n+\frac{1}{2}}, \tag{3.8}$$

$$\mu^{n+\frac{1}{2}} = \mathcal{L}\phi^{n+\frac{1}{2}} + \sum_{i=1}^{m} \frac{r_i^{n+\frac{1}{2}}}{G_i(\int_\Omega F_i(\phi^{\star,n+\frac{1}{2}})d\boldsymbol{x})}F_i'(\phi^{\star,n+\frac{1}{2}}), \tag{3.9}$$

$$\begin{aligned}&\frac{G_i^{-1}(r_i^{n+1}) - G_i^{-1}(r_i^n)}{\delta t}\\ &= \frac{r_i^{n+\frac{1}{2}}}{G_i(\int_\Omega F_i(\phi^{\star,n+\frac{1}{2}})d\boldsymbol{x})}(F_i'(\phi^{\star,n+\frac{1}{2}}), \frac{\phi^{n+1}-\phi^n}{\delta t}), \quad i = 1, 2, \ldots, m.\end{aligned} \tag{3.10}$$

where $g^{\star,n+\frac{1}{2}} = \frac{3}{2}g^n - \frac{1}{2}g^{n-1}$ for any sequence $\{g^n\}$.

Taking inner product of Eqs. (3.8) with $\mu^{n+\frac{1}{2}}$, of Eq. (3.9) with $\frac{\phi^{n+1}-\phi^n}{\delta t}$ and combining with Eqs. (3.10), we derive the following energy dissipative law for scheme (3.8)–(3.10):

$$\tilde{E}(\phi^{n+1}) - \tilde{E}(\phi^n) = -\delta t(\mathcal{G}\mu^{n+\frac{1}{2}}, \mu^{n+\frac{1}{2}}),$$

where $\tilde{E}(\phi^k) = \int_\Omega \frac{1}{2}\mathcal{L}\phi^k\cdot\phi^k d\boldsymbol{x} + \sum_{i=1}^m G_i^{-1}(r_i^k)$.

The scheme (3.8)–(3.10) is also a weakly coupled nonlinear system. Below we show how to implement it efficiently. Similarly as in the last section, we rewrite (3.8) as (2.14), set

$$\xi_i^{n+\frac{1}{2}} = \frac{r_i^{n+\frac{1}{2}}}{G_i(\int_\Omega F_i(\phi^{\star,n+\frac{1}{2}})d\boldsymbol{x})}, \ i = 1, 2, \ldots, m, \tag{3.11}$$

and express $\phi^{n+\frac{1}{2}}$ and $\mu^{n+\frac{1}{2}}$ as

$$\phi^{n+\frac{1}{2}} = \phi_1^{n+\frac{1}{2}} + \sum_{i=1}^{m} \xi_i^{n+\frac{1}{2}}\phi_{i,2}^{n+\frac{1}{2}}, \tag{3.12}$$

and

$$\mu^{n+\frac{1}{2}} = \mu_1^{n+\frac{1}{2}} + \sum_{i=1}^{m} \xi_i^{n+\frac{1}{2}}\mu_{i,2}^{n+\frac{1}{2}}. \tag{3.13}$$

Plugging the above in (3.8)–(3.9), we find that $(\phi_1^{n+\frac{1}{2}}, \mu_1^{n+\frac{1}{2}})$ and $(\phi_{i,2}^{n+\frac{1}{2}}, \mu_{i,2}^{n+\frac{1}{2}})$ can be determined by solving the following decoupled linear systems with constant coefficients:

$$\frac{\phi_1^{n+\frac{1}{2}} - \phi^n}{\frac{1}{2}\delta t} = -\mathcal{G}\mu_1^{n+\frac{1}{2}}, \tag{3.14}$$

$$\mu_1^{n+\frac{1}{2}} = \mathcal{L}\phi_1^{n+\frac{1}{2}}, \tag{3.15}$$

and

$$\frac{\phi_{i,2}^{n+\frac{1}{2}}}{\frac{1}{2}\delta t} = -\mathcal{G}\mu_{i,2}^{n+\frac{1}{2}}, \tag{3.16}$$

$$\mu_{i,2}^{n+\frac{1}{2}} = \mathcal{L}\phi_{i,2}^{n+\frac{1}{2}} + F_i'(\phi^{\star,n+\frac{1}{2}}). \tag{3.17}$$

Once $(\phi_1^{n+\frac{1}{2}}, \mu_1^{n+\frac{1}{2}})$ and $(\phi_{i,2}^{n+\frac{1}{2}}, \mu_{i,2}^{n+\frac{1}{2}})$ are known, we plug Eqs. (3.11) and (3.12) into (3.10) to obtain a coupled nonlinear algebraic system for $\xi_i^{n+\frac{1}{2}}$ $(i = 1, 2, \ldots, m)$ which can be solved by using a Newton iteration with 1 as initial guess for $\xi_i^{n+\frac{1}{2}}$ $(i = 1, 2, \ldots, m)$. Finally, we obtain (ϕ^{n+1}, μ^{n+1}) from (3.12) and (3.13).

3.2. Extensions to gradient systems with multiple components

We consider multiple-components phase field models which play an important role in describing three material components [17,18]. We introduce ϕ_i $(i = 1, 2, \ldots, m)$ be the ith phase variables. A special form of total free energy for multi-phase system is formulated as

$$E(\phi_1, \phi_2, \ldots, \phi_m) = \sum_{i,j=1}^{m} \int_\Omega \mathcal{L}\phi_i \cdot \phi_j d\boldsymbol{x} + \int_\Omega F(\phi_1, \phi_2, \ldots, \phi_m) d\boldsymbol{x}, \tag{3.18}$$

where $\mathcal{L}$ is a self-adjoint nonnegative linear operator, and the constant matrix d_{ij} is symmetric positive definite. $F(\phi_1, \phi_2, \ldots, \phi_m)$ is nonlinear potential. We derive the multi-components phase field model by taking variational derivative with respect to (3.18),

$$\begin{cases} \partial_t \phi_i = \mathcal{G}\mu_i \\ \mu_i = \mathcal{L}\phi_i + f_i \end{cases}, \qquad i = 1, 2, \ldots, m, \tag{3.19}$$

with suitable boundary conditions.

Taking inner product of Eq. (3.19) with μ_i and $\partial_t \phi_i$ respectively for $i = 1, 2, \ldots, m$, integrating by parts and summing up these three equalities, we obtain the following energy dissipative law:

$$\frac{d}{dt} E(\phi_1, \phi_2, \ldots, \phi_m) = -\sum_{i=1}^{m} (\mathcal{G}\mu_i, \mu_i). \tag{3.20}$$

We rewrite energy (3.18) to the following form

$$E(\phi_1, \phi_2, \ldots, \phi_m) = \sum_{i=1}^{m} \int_\Omega \mathcal{L}\phi_i \cdot \phi_i d\boldsymbol{x} + G^{-1}\{G(\int_\Omega F(\phi_1, \phi_2, \ldots, \phi_m) d\boldsymbol{x})\}. \tag{3.21}$$

Introducing a new SAV

$$r(t) = G(\int_\Omega F(\phi_1, \phi_2, \ldots, \phi_m) d\boldsymbol{x}), \tag{3.22}$$

then the system (3.19) is reformulated as

$$\begin{aligned} &\partial_t \phi_i = \mathcal{G}\mu_i, \quad i = 1, 2, \ldots, m, \\ &\mu_i = \mathcal{L}\phi_i + \frac{r}{G(\int_\Omega F(\phi_1, \phi_2, \ldots, \phi_m) d\boldsymbol{x})} f_i, \quad i = 1, 2, \ldots, m, \\ &\frac{d}{dt} G^{-1}(r) = \frac{r}{G(\int_\Omega F(\phi_1, \phi_2, \ldots, \phi_m) d\boldsymbol{x})} \sum_{i=1}^{3} (f_i, \partial_t \phi_i). \end{aligned} \tag{3.23}$$

Then a Crank–Nicolson G-SAV scheme for system (3.23) is

$$\begin{aligned}
&\frac{\phi_i^{n+1}-\phi_i^n}{\delta t} = \mathcal{G}\mu_i^{n+\frac{1}{2}}, \quad i=1,\dots,m,\\
&\mu_i^{n+\frac{1}{2}} = \mathcal{L}\phi_i^{n+\frac{1}{2}} + \frac{r^{n+\frac{1}{2}}}{G(\int_\Omega F(\phi_1^{\star,n+\frac{1}{2}},\phi_2^{\star,n+\frac{1}{2}},\dots,\phi_m^{\star,n+\frac{1}{2}})d\boldsymbol{x})} f_i^{\star,n+\frac{1}{2}}, \quad i=1,2,\dots,m,\\
&\frac{(G^{-1}(r))^{n+1}-(G^{-1}(r))^n}{\delta t} = \frac{r^{n+\frac{1}{2}}}{G(\int_\Omega F(\phi_1^{\star,n+\frac{1}{2}},\phi_2^{\star,n+\frac{1}{2}},\dots,\phi_m^{\star,n+\frac{1}{2}})d\boldsymbol{x})}\sum_{i=1}^m (f_i^{\star,n+\frac{1}{2}}, \frac{\phi_i^{n+1}-\phi_i^n}{\delta t}),
\end{aligned} \tag{3.24}$$

where $f_i^{*,n+\frac{1}{2}} = \frac{1}{2}(3f_i^n - f_i^{n-1})$ and $\phi^{*,n+\frac{1}{2}} = \frac{1}{2}(3\phi^n - \phi^{n-1})$.

Taking inner product of Eq. (3.24) with $\mu_i^{n+\frac{1}{2}}$, $\frac{\phi_i^{n+1}-\phi_i^n}{\delta t}$ for $i=1,2,\dots,m$, summing up these three equalities and combining the third equation of (3.24), we derive the following energy dissipative law for scheme (3.24):

$$\tilde{E}(\phi_1^{n+1},\phi_2^{n+1},\dots,\phi_m^{n+1}) - \tilde{E}(\phi_1^n,\phi_2^n,\dots,\phi_m^n) = -\sum_{i=1}^m (\mathcal{G}\mu_i^{n+\frac{1}{2}}, \mu_i^{n+\frac{1}{2}}),$$

where $\tilde{E}(\phi^k) = \int_\Omega \sum_{i=1}^m \frac{1}{2}\mathcal{L}\phi_i^k \cdot \phi_i^k d\boldsymbol{x} + G^{-1}(r^k)$.

The scheme (3.24) can also efficiently implemented as follows. Setting

$$\xi^{n+\frac{1}{2}} = \frac{r^{n+\frac{1}{2}}}{G(\int_\Omega F(\phi_1^{\star,n+\frac{1}{2}},\phi_2^{\star,n+\frac{1}{2}},\dots,\phi_m^{\star,n+\frac{1}{2}})d\boldsymbol{x})},$$

and writing

$$\phi_i^{n+\frac{1}{2}} = \phi_{i,1}^{n+\frac{1}{2}} + \xi^{n+\frac{1}{2}}\phi_{i,2}^{n+\frac{1}{2}}, \ \mu_i^{n+\frac{1}{2}} = \mu_{i,1}^{n+\frac{1}{2}} + \xi^{n+\frac{1}{2}}\mu_{i,2}^{n+\frac{1}{2}}, \tag{3.25}$$

in the first two equations of (3.24), we find that $(\phi_i^{n+\frac{1}{2}}, \mu_i^{n+\frac{1}{2}})$ $(i=1,2,\dots,m)$ can be determined as follows:

$$\frac{\phi_{i,1}^{n+\frac{1}{2}}-\phi_i^n}{\frac{1}{2}\delta t} = \mathcal{G}\mu_{i,1}^{n+\frac{1}{2}}, \tag{3.26}$$

$$\mu_{i,1}^{n+\frac{1}{2}} = \mathcal{L}\phi_{i,1}^{n+\frac{1}{2}}, \quad i=1,2,\dots,m, \tag{3.27}$$

and

$$\frac{\phi_{i,2}^{n+\frac{1}{2}}}{\frac{1}{2}\delta t} = \mathcal{G}\mu_{i,2}^{n+\frac{1}{2}}, \tag{3.28}$$

$$\mu_{i,2}^{n+\frac{1}{2}} = \mathcal{L}\phi_{i,2}^{n+\frac{1}{2}} + f_i^{\star,n+\frac{1}{2}}. \tag{3.29}$$

Once $(\phi_{i,1}^{n+\frac{1}{2}}, \phi_{i,2}^{n+\frac{1}{2}})$ are solved, we plug (3.25) into the third equation of (3.24) to obtain a nonlinear algebraic equation for $\xi^{n+\frac{1}{2}}$ which can be solved by a Newton iteration with 1 as initial guess. Finally we obtain (ϕ^{n+1}, μ^{n+1}) using (3.25).

4. Numerical results

In this section, we shall present several numerical experiments to validate the stability and demonstrate the convergence rates of the G-SAV approach, and compare the performance of the G-SAV approaches. In all numerical examples below, we assume periodic boundary conditions and use a Fourier Spectral method in space. The default computational domain is $[-\pi,\pi)^2$.

4.1. Validation and comparison using the first G-SAV approach

We consider the Allen–Cahn [19] and Cahn–Hilliard [20,21] equation. The total free energy of Allen–Cahn and Cahn–Hilliard equation is

$$E_{tot} = \int_\Omega \frac{1}{2}|\nabla\phi|^2 + F(\phi)d\boldsymbol{x},$$

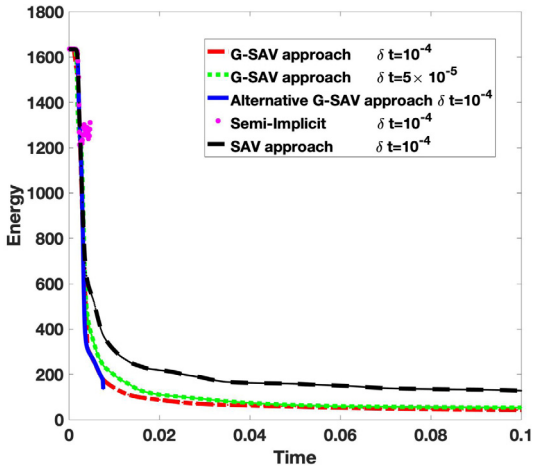

Fig. 4.1. Evolutions of original energy computed by various numerical schemes including the first G-SAV approach (2.11)–(2.13), alternative G-SAV approach, semi-implicit and original SAV approach.

where $F(\phi) = \frac{1}{4\epsilon^2}(\phi^2 - 1)^2$ is the double well potential. The form of chemical potential in (2.2) is

$$\mu = -\Delta\phi + F'(\phi),$$

with $\mathcal{G} = I$ for Allen–Cahn equation and $\mathcal{G} = -\Delta$ for Cahn–Hilliard equation.

We use 128 modes in each direction in our Fourier Spectral method so that the spatial discretization errors are negligible compared with time discretization error.

4.1.1. Comparison between various SAV approaches and the semi-implicit approach

In this subsection, we consider the Cahn–Hilliard equation with the interface width parameter as $\epsilon^2 = 0.005$. Evolutions of energy with respect to time computed by various approaches are depicted in Fig. 4.1 with initial condition (4.1) and $G = C\ln x$, $G^{-1} = e^{x/C}$ where constant C is set to be 10^3. We observe that at $\delta t = 10^{-4}$, the original energy using the scheme (2.50)–(2.52) by the alternative approach and the usual semi-implicit scheme (i.e., (2.50)–(2.51) with $\frac{r^{*,n+1/2}}{G(\int_\Omega F(\phi^{*,n+1/2})d\boldsymbol{x}+C_0)}$ replaced by 1) are no longer dissipative, indicating that the modified energy, which is guaranteed to be dissipative, deviates from the original energy so the numerical solution is no longer very accurate. On the other hand, the original energy computed with the schemes based on the first G-SAV approach and the original SAV approach are still energy dissipative.

The above results indicate that the "effective" accuracy of the scheme (2.50)–(2.52) by the alternative approach is very similar to the usual semi-implicit scheme, and it is not as robust as the schemes by the original SAV and the first G-SAV approach in dealing with models with stiff nonlinear terms.

4.1.2. *Comparison of the first G-SAV approach with different G*

We consider the 2D Cahn–Hilliard equation and choose a random initial condition

$$\phi(x, y) = 0.03 + 0.001\,\mathrm{rand}(x, y), \tag{4.1}$$

where $\mathrm{rand}(x, y)$ represents random data between $[-1, 1]^2$.

In Fig. 4.2, we plot the dynamic evolution of phase separation for Cahn–Hilliard equation by using second-order BDF schemes of the first G-SAV approach with different G with $\delta t = 10^{-5}$ and the second-order exponential time differencing Runge–Kutta scheme (ETDRK2) [22] with $\delta t = 10^{-5}$. We observe that the second-order G-SAV schemes and ETDRK2 lead to indistinguishable ϕ in Fig. 4.2. In Fig. 4.3, the evolutions of original and modified energy computed by second-order G-SAV schemes and ETDRK2 are depicted. No visible difference are observed.

4.1.3. *Convergence rate with given exact solution*

We test the convergence rate of BDF2 and Crank–Nicolson schemes of the first G-SAV approach with two different G functions for the (forced) 2D Allen–Cahn equation with the exact solution

$$\phi(x, y, t) = \left(\frac{\sin(2x)\cos(2y)}{4} + 0.48\right)\left(1 - \frac{\sin^2(t)}{2}\right), \tag{4.2}$$

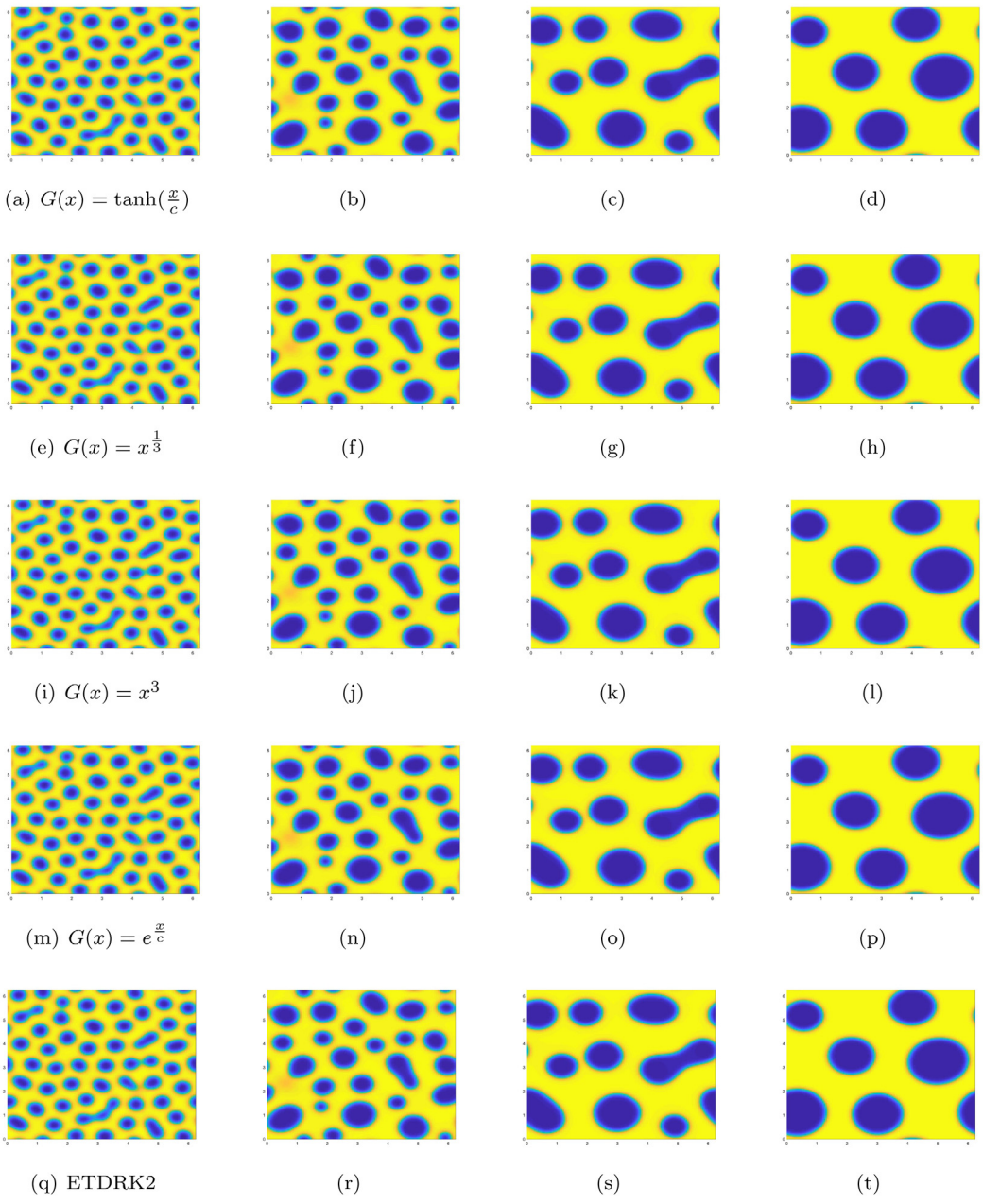

Fig. 4.2. The 2D dynamical evolutions of the phase variable ϕ at $t = 0.0025, 0.01, 0.04, 0.1$ for the Cahn–Hilliard equation with parameters $\epsilon^2 = 0.005$ computed by BDF2 scheme of the first G-SAV approach and ETDRK2 with $\delta t = 10^{-5}$. The constant c is equal to 10^4 for tanh and mapped exponential SAV approaches.

where interface width is $\epsilon^2 = 0.01$. In Tables 4.1 and 4.2, we show the L^∞ errors of ϕ with different time steps computed by BDF2 and Crank–Nicolson G-SAV schemes with $G(x) = \tanh(\frac{x}{10^4})$ and $G(x) = x^3$. We observe that both choices lead to second-order accuracy and $G = \tanh(\frac{x}{10^4})$ leads to slightly more accurate results than $G = x^3$.

4.2. Validation of the second G-SAV approach

The main advantages of the second G-SAV approach are that (i) it only requires the total free energy to be bounded from below; and (ii) it is shown that $G^{-1}(r^{n+1})$ to be bounded below. We use the schemes based on the second G-SAV approach to compute the Allen–Cahn equation with the exact solution given by (4.2) with $\epsilon^2 = 0.01$. In Table 4.3, we show

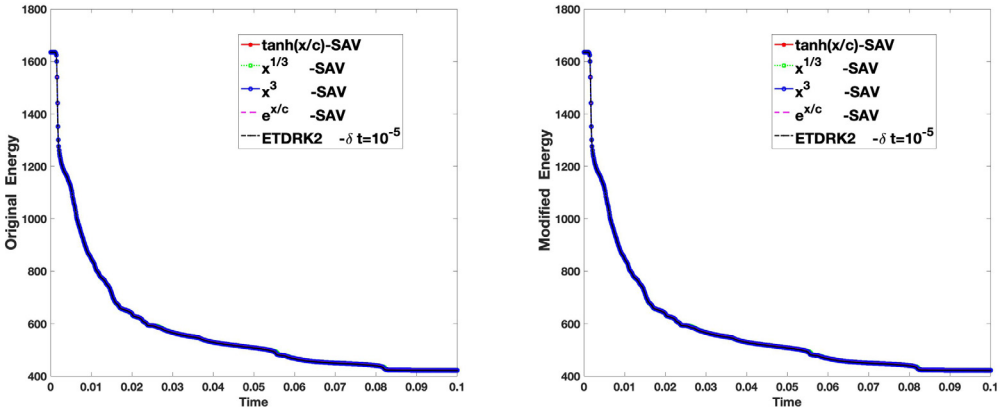

Fig. 4.3. Left: Evolutions of original energy by using various SAV approaches and ETDRK2 for Fig. 4.2; Right: Evolutions of the corresponding modified energy of the first G-SAV approach.

Table 4.1
Accuracy test: The L^∞ errors of ϕ at $t = 0.1$ for the Allen–Cahn equation computed by BDF2 and Crank–Nicolson version of G-SAV scheme (2.11)–(2.13) with $G(x) = \tanh(\frac{x}{10^4})$.

δt	$BDF2 - \tanh(\frac{x}{c})$	Order	$CN2 - \tanh(\frac{x}{c})$	Order
1×10^{-2}	$2.65E(-2)$	–	$2.86E(-2)$	–
1×10^{-3}	$7.85E(-4)$	–	$8.35E(-4)$	–
8×10^{-4}	$5.41E(-4)$	–	$5.77E(-4)$	–
4×10^{-4}	$1.35E(-4)$	1.98	$1.46E(-4)$	2.00
2×10^{-4}	$3.37E(-5)$	1.99	$3.66E(-5)$	2.00
1×10^{-4}	$8.41E(-6)$	1.99	$9.16E(-6)$	2.00
5×10^{-5}	$2.10E(-6)$	2.00	$2.29E(-6)$	2.00
2.5×10^{-5}	$5.24E(-7)$	1.99	$5.73E(-7)$	2.00
1.25×10^{-5}	$1.31E(-7)$	2.00	$1.43E(-7)$	2.00

Table 4.2
Accuracy test: The L^∞ errors of ϕ at $t = 0.1$ for the Allen–Cahn equation computed by BDF2 and Crank–Nicolson version of G-SAV scheme (2.11)–(2.13) with $G(x) = x^3$.

δt	$BDF2 - x^3$	Order	$CN2 - x^3$	Order
1×10^{-2}	$3.72E(-2)$	–	$3.99E(-2)$	–
1×10^{-3}	$2.11E(-3)$	–	$2.03E(-3)$	–
8×10^{-4}	$1.47E(-3)$	–	$1.42E(-3)$	–
4×10^{-4}	$3.74E(-4)$	1.97	$3.70E(-4)$	1.94
2×10^{-4}	$9.37E(-5)$	1.99	$9.48E(-5)$	1.96
1×10^{-4}	$2.33E(-5)$	2.00	$2.39E(-5)$	1.98
5×10^{-5}	$5.84E(-6)$	1.99	$6.00E(-6)$	1.99
2.5×10^{-5}	$1.45E(-6)$	2.00	$1.50E(-6)$	2.00
1.25×10^{-5}	$3.64E(-7)$	1.99	$3.77E(-7)$	1.99

Table 4.3
Accuracy test: The L^∞ errors of ϕ at $t = 0.1$ for the Allen–Cahn equation computed by BDF2 and Crank–Nicolson G-SAV scheme (2.24)–(2.27) with $G(x) = x^3$.

δt	$BDF2 - x^3$	Order	$CN2 - x^3$	Order
1×10^{-2}	$2.61E(-2)$	–	$1.77E(-2)$	–
1×10^{-3}	$7.78E(-4)$	–	$1.96E(-4)$	–
8×10^{-4}	$5.37E(-4)$	–	$1.30E(-4)$	–
4×10^{-4}	$1.34E(-4)$	2.00	$3.02E(-5)$	2.10
2×10^{-4}	$3.34E(-5)$	2.00	$7.24E(-6)$	2.06
1×10^{-4}	$8.34E(-6)$	2.00	$1.76E(-6)$	2.04
5×10^{-5}	$2.08E(-6)$	2.00	$4.37E(-7)$	2.00
2.5×10^{-5}	$5.20E(-7)$	2.00	$1.08E(-7)$	2.01
1.25×10^{-5}	$1.30E(-7)$	2.00	$2.73E(-8)$	1.98

the L^∞ errors of ϕ with different time steps computed by BDF2 and Crank–Nicolson version of the scheme (2.24)–(2.27) with $G(x) = x^3$. It is observed from Table 4.3 that accurate results can be obtained with quite large time steps.

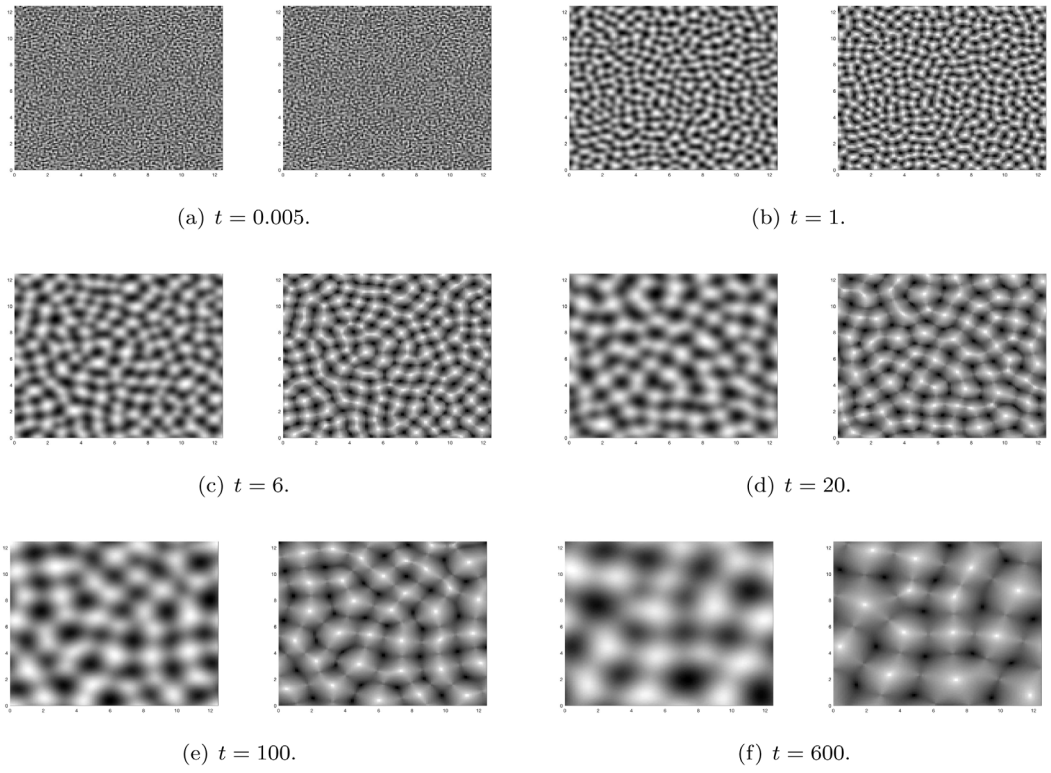

(a) $t = 0.005$. (b) $t = 1$.

(c) $t = 6$. (d) $t = 20$.

(e) $t = 100$. (f) $t = 600$.

Fig. 4.4. The isolines of the numerical solutions of the height function ϕ and its Laplacian $\Delta\phi$ for the model without slope selection with random initial condition. For each subfigure, the left is ϕ and the right is $\Delta\phi$. Snapshots are taken at $t = 0.005, 1, 6, 20, 100, 600$, respectively.

Next we apply the second G-SAV approach to the molecular beam epitaxial (MBE) without slope selection [23]. The total free energy is $E(\phi) = \int_\Omega \frac{\epsilon^2}{2}|\Delta\phi|^2 + F(\phi)d\boldsymbol{x}$, and the L^2 gradient flow is

$$\phi_t = -M\frac{\delta E(\phi)}{\delta\phi} = -M\big(\epsilon^2\Delta^2\phi + F'(\phi)\big), \tag{4.3}$$

where M is a mobility constant, and $F'(\phi) = \nabla\cdot\left(\frac{\nabla\phi}{1+|\nabla\phi|^2}\right)$.

Since the nonlinear potential $F(\phi) = -\frac{1}{2}\ln(1+|\nabla\phi|^2)$ is not bounded from below, the original SAV approach and the first G-SAV approach cannot be directly applied. In [10], we had to add a small linear part $\delta\int_\Omega \frac{\epsilon^2}{2}|\Delta\phi|^2 d\boldsymbol{x}$ to the nonlinear potential to make it bounded from below. However, if we use the G-SAV approach, we just need to choose a function G, e.g., $G(x) = \tanh(\frac{x}{C})$, with the domain of definition $\mathbb{R}$.

We simulated the coarsening dynamical process of MBE model with

$$\epsilon = 0.03,\ \delta t = 10^{-2},\ M = 1,\ \Omega = [0, 2\pi)^2, \tag{4.4}$$

using the second kind of BDF2 G-SAV (2.24)–(2.27) scheme. A random initial condition varying from -0.001 to 0.001 is used.

It is well-known that the total free energy decays with rate behaving like $-88\log(t) - 124$. The computed free energy which is consistent with this rate is depicted in Fig. 4.5. The coarse dynamic process are plotted in Fig. 4.4 which are visibly consistent with numerical results in [10,24].

4.3. Validation of the third G-SAV approach

The main advantage of the third G-SAV approach is that it dissipates the original energy. We apply the third G-SAV approach (2.39)–(2.42) for the Allen–Cahn equation with interface width $\epsilon^2 = 0.05$ by using time step $\delta t = 10^{-4}$. The initial condition is chosen as random data (4.1). We plot the evolution of the original energy in Fig. 4.6 and observe that it indeed decays with time.

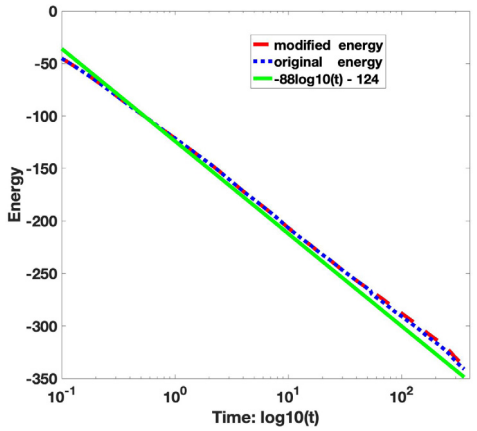

Fig. 4.5. The evolution of computed free energy for MBE model without slope selection.

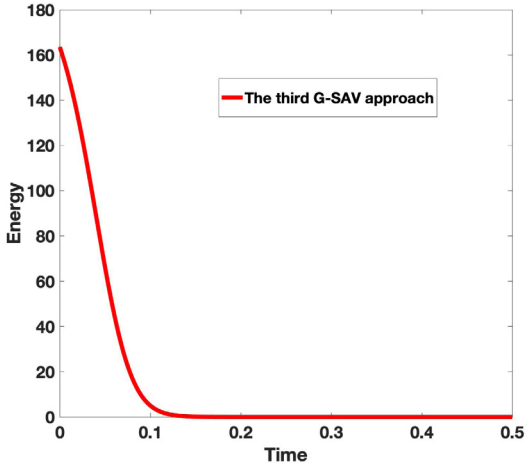

Fig. 4.6. Evolution of the original energy for Allen–Cahn equation computed by the third G-SAV approach (2.39)–(2.42).

4.4. Application of the first G-SAV approach to a block copolymer model

As an example of gradient flow with multiple components, we consider the block copolymer (BCP) model [25,26] in the form

$$u_t = M_u \Delta \frac{\delta E(u,v)}{\delta u}, \tag{4.5}$$

$$v_t = M_v \Delta \frac{\delta E(u,v)}{\delta v}, \tag{4.6}$$

with the total free energy

$$E_{\epsilon_u,\epsilon_v}(u,v) = \int_\Omega \frac{\epsilon_u^2}{2}|\nabla u|^2 + \frac{\epsilon_v^2}{2}|\nabla v|^2 + W(u,v) + \frac{\sigma}{2}|(-\Delta)^{-\frac{1}{2}}(v-\overline{v})|^2 d\boldsymbol{x}, \tag{4.7}$$

where

$$W(u,v) = \frac{(u^2-1)^2}{4} + \frac{(v^2-1)^2}{4} + \alpha uv + \beta uv^2 + \gamma u^2 v.$$

The problem is supplemented with periodic boundary conditions. One can easily check that

$$\frac{\delta E(u,v)}{\delta u} = -\epsilon_u^2 \Delta u + \frac{\delta W}{\delta u} = \mu_u, \quad \frac{\delta E(u,v)}{\delta v} = -\epsilon_u^2 \Delta v + \frac{\delta W}{\delta v} - \sigma \Delta^{-1}(v-\overline{v}) = \mu_v.$$

This coupled Cahn–Hilliard system models the dynamics of BCP particles surrounded with homopolymer. The order parameter u describes these two components in the interval $[-1, 1]$, -1 represents the homopolymer rich domain and

1 is the BCP-rich domain. The order parameter v describes micro separation inside the BCP domain which also acquires values from interval $[-1, 1]$ with the end points corresponding to A-type BCP and B-type BCP. ϵ_u and ϵ_v are diffusive interface parameters, $\bar{v}$ is the average of v, M_u and M_v are mobility constants, and $\alpha, \beta, \gamma, \sigma$ are modeling constants. The non-local operator $(-\Delta)^{-\frac{1}{2}}$ is defined through the spectral decomposition of the Laplace operator.

The system (4.5)–(4.6) is a gradient system with two components. The G-SAV approach for general gradient systems with multi-components is described in Section 3. For the reader's convenience, we write down below a second-order BDF scheme based on the first G-SAV approach for (4.5)–(4.6).

We define a new variable $r = G(\int_\Omega W(u, v)d\boldsymbol{x})$ where G is an invertible function and rewrite the total free energy as

$$E_{\epsilon_u,\epsilon_v}(u, v) = \int_\Omega \frac{\epsilon_u^2}{2}|\nabla u|^2 + \frac{\epsilon_v^2}{2}|\nabla v|^2 + \frac{\sigma}{2}|(-\Delta)^{-\frac{1}{2}}(v - \bar{v})|^2 d\boldsymbol{x} + G^{-1}\{G(\int_\Omega W(u, v)d\boldsymbol{x})\}. \tag{4.8}$$

Then, the second-order BDF G-SAV scheme is as follows:

$$\frac{3u^{n+1} - 4u^n + u^{n-1}}{2\delta t} = M_u\Delta\mu_u^{n+1}, \tag{4.9}$$

$$\mu_u^{n+1} = -\epsilon_u^2\Delta u^{n+1} + (\frac{\delta W}{\delta u})^{\dagger,n}\frac{r^{n+1}}{G(\int_\Omega W(u^{\dagger,n}, v^{\star,n})d\boldsymbol{x})}, \tag{4.10}$$

$$\frac{3v^{n+1} - 4v^n + v^{n-1}}{2\delta t} = M_v\Delta\mu_v^{n+1}, \tag{4.11}$$

$$\mu_v^{n+1} = -\epsilon_v^2\Delta v^{n+1} + (\frac{\delta W}{\delta v})^{\dagger,n}\frac{r^{n+1}}{G(\int_\Omega W(u^{\dagger,n}, v^{\dagger,n})d\boldsymbol{x})} - \sigma\Delta^{-1}(v^{n+1} - \bar{v}), \tag{4.12}$$

$$3G^{-1}(r^{n+1}) - 4G^{-1}(r^n) + G^{-1}(r^{n-1}), \tag{4.13}$$
$$= \frac{r^{n+1}}{G(\int_\Omega W(u^{\dagger,n}, v^{\dagger,n})d\boldsymbol{x})}\{((\frac{\delta W}{\delta u})^{\dagger,n}, 3u^{n+1} - 4u^n + u^{n-1}) + ((\frac{\delta W}{\delta v})^{\dagger,n}, 3v^{n+1} - 4v^n + v^{n-1})\}.$$

where $f^{\dagger,n} = 2f^n - f^{n-1}$ for any function f. The G-SAV scheme (4.9)–(4.13) is unconditionally energy dissipative and can be solved following the general approach for the scheme (3.24) in Section 3. Note that the nonlocal term, with periodic boundary condition does not pose any additional difficulty.

Now we present some numerical experiments to simulate the annealing process [25,26] of block copolymer and detect its morphology transformations. The parameters of the coupled Cahn–Hilliard system are chosen as

$$\epsilon_u = 0.075 \quad \epsilon_v = 0.02 \quad \sigma = 10 \quad \alpha = 0.1 \quad \beta = -0.75 \quad \gamma = 0, \tag{4.14}$$

and domain is set to be $[-1, 1]$ with periodic boundary conditions. The initial conditions are

$$u(t = 0) = \text{rand}(x, y), \quad v(t = 0) = \text{rand}(x, y), \tag{4.15}$$

where the rand(x, y) is a uniformly distributed random function in $[-1, 1]^2$ with zero mean. We shall use the yellow bulk to represent the A-BCP particles, and blue bulk to represent the B-BCP particles. The numerical solutions in Figs. 4.8 and 4.9 are computed by the G-SAV scheme (4.9)–(4.13) with $G = e^{x/C}$ and $G = \sqrt{x + C}$ with time step $\delta t = 5 \times 10^{-5}$. We observe that the contours of numerical solution are indistinguishable by using these two different G. Phase variable u represents the confined surface for BCP particles. While variable v describes the dynamic process of morphological transformation for BCP particles. From Fig. 4.8 we observe that the striped ellipsoids gradually appear. If we only change the parameter ϵ_v a litter bit larger and given the following parameters

$$\epsilon_u = 0.075 \quad \epsilon_v = 0.05 \quad \sigma = 10 \quad \alpha = 0.1 \quad \beta = -0.75 \quad \gamma = 0, \tag{4.16}$$

We depict numerical results at various time in Fig. 4.9. Similarly in Fig. 4.9, striped ellipsoids are also formed finally. Both final morphologies in Figs. 4.8 and 4.9 are consistent with the experimental results depicted in Fig. 4.7 which also are observed in numerical simulations in [25,26].

5. Concluding remarks

The application of the original SAV approach is somewhat limited by the requirement that the nonlinear potentials are bounded from below, and the scheme constructed using the original SAV approach is only energy stable with respect to a modified energy. We proposed in this paper three G-SAV approaches which, respectively, allow a range of choices for the function in the definition of the SAV, extend the applicability of the original SAV approach, and lead to unconditionally energy stable schemes with respect to the original energy, while keeping other essential advantages of the original SAV

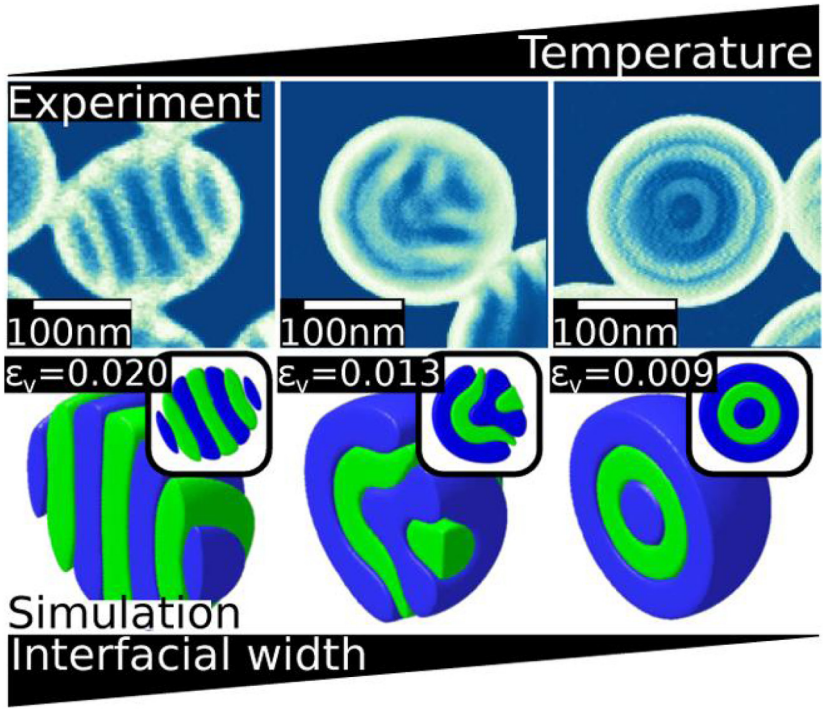

Fig. 4.7. Experimental results and simulations at various temperature in [25,26].

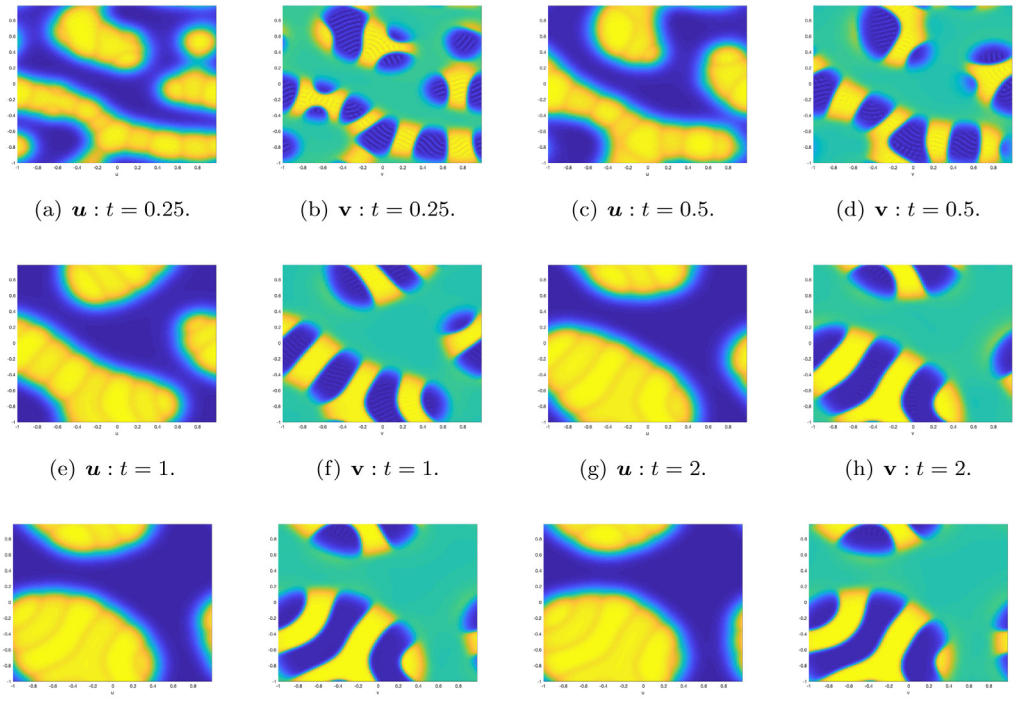

(a) $\boldsymbol{u} : t = 0.25$. (b) $\mathbf{v} : t = 0.25$. (c) $\boldsymbol{u} : t = 0.5$. (d) $\mathbf{v} : t = 0.5$.

(e) $\boldsymbol{u} : t = 1$. (f) $\mathbf{v} : t = 1$. (g) $\boldsymbol{u} : t = 2$. (h) $\mathbf{v} : t = 2$.

(i) $\boldsymbol{u} : t = 3$. (j) $\mathbf{v} : t = 3$. (k) $\boldsymbol{u} : t = 5$. (l) $\mathbf{v} : t = 5$.

Fig. 4.8. Evolution of the phase variable $\mathbf{u}, \mathbf{v}$ for the Coupled-BCP model with the initial condition (4.15) and $G = e^{x/C}$ with $C = 10^4$. (For interpretation of the references to color in this figure legend, the reader is referred to the web version of this article.)

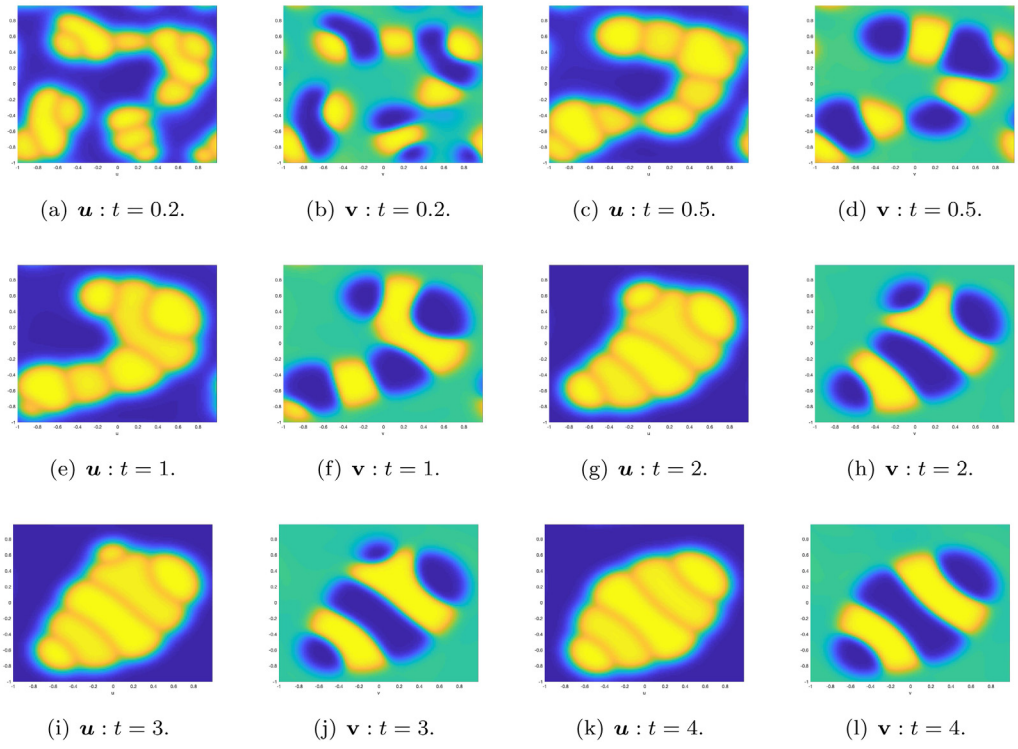

(a) $\boldsymbol{u} : t = 0.2$. (b) $\mathbf{v} : t = 0.2$. (c) $\boldsymbol{u} : t = 0.5$. (d) $\mathbf{v} : t = 0.5$.

(e) $\boldsymbol{u} : t = 1$. (f) $\mathbf{v} : t = 1$. (g) $\boldsymbol{u} : t = 2$. (h) $\mathbf{v} : t = 2$.

(i) $\boldsymbol{u} : t = 3$. (j) $\mathbf{v} : t = 3$. (k) $\boldsymbol{u} : t = 4$. (l) $\mathbf{v} : t = 4$.

Fig. 4.9. Evolution of the phase variable $\mathbf{u}, \mathbf{v}$ for the Coupled-BCP model with the initial condition (4.15) and $G = \sqrt{x + C}$ with $C = 10$. (For interpretation of the references to color in this figure legend, the reader is referred to the web version of this article.)

approach. In particular, the first G-SAV approach includes the original SAV approach as a special case with $G(x) = \sqrt{x + C}$ and a slight modification.

We presented several numerical comparisons and simulations for various gradient systems to validate the effectiveness and accuracy of the proposed G-SAV approaches. Below are some recommendations as to the choice of G-SAV approaches and of time discretization schemes:

- For problems with nonlinear part of the free energy bounded from below, the original SAV approach is still the method of choice as it does not involve any nonlinear algebraic equations. While we are unable to prove that $(G^{-1}(r))^n$ in the first G-SAV approach has a lower bound, our numerical results indicate that, when the time step is not too large, $(G^{-1}(r))^n$ are well bounded from below and lead to very good numerical results for a range of G.
- If the nonlinear part of the free energy cannot be shown to be bounded from below, one can use the second or third G-SAV approach.
- If it is important to ensure that the original energy to be dissipative, then the third G-SAV approach is a good choice.
- For dissipative gradient systems, BDF versions of the G-SAV approaches should be used as it provides additional dissipation which helps to damp initial errors.
- For conservative gradient systems such as nonlinear Schrödinger equations, the Crank–Nicolson version of the G-SAV approaches should be used as it is the only choice which conserves the energy.

Although we considered only time-discretization schemes in this paper, since the stability proofs are all based on variational formulations with the same space for trial and test functions, we can combine these semi-discrete schemes with any consistent Galerkin type approximations in space to construct fully discrete energy stable schemes.

References

[1] Qiang Du, Xiaobing Feng, The phase field method for geometric moving interfaces and their numerical approximations, 2019, arXiv preprint arXiv:1902.04924.
[2] Jie Shen, Jie Xu, Jiang Yang, The scalar auxiliary variable (SAV) approach for gradient flows, J. Comput. Phys. 353 (2018) 407–416.
[3] Jie Shen, Jie Xu, Jiang Yang, A new class of efficient and robust energy stable schemes for gradient flows, SIAM Rev. 61 (3) (2019) 474–506.
[4] Xiaofeng Yang, Linear, first and second-order, unconditionally energy stable numerical schemes for the phase field model of homopolymer blends., J. Comput. Phys. 327 (2016).
[5] Qing Cheng, Jie Shen, Multiple scalar auxiliary variable (MSAV) approach and its application to the phase-field vesicle membrane model, SIAM J. Sci. Comput. 40 (6) (2018) A3982–A4006.

[6] Georgios Akrivis, Buyang Li, Dongfang li, Energy-decaying extrapolated RK–SAV Methods for the Allen–Cahn and Cahn–Hilliard Equations, SIAM J. Sci. Comput. 41 (6) (2019) A3703–A3727.
[7] Jun Zhang, Xiaofeng Yang, Decoupled, non-iterative, and unconditionally energy stable large time stepping method for the three-phase Cahn-Hilliard phase-field model, J. Comput. Phys. 404 (2020) 109115, 26.
[8] Yang Zhiguo, Dong Suchuan, A roadmap for discretely energy-stable schemes for dissipative systems based on a generalized auxiliary variable with guaranteed positivity, J. Comput. Phys. 404 (2020).
[9] Qing Cheng, Chun Liu, Jie Shen, A new Lagrange multiplier approach for gradient flows, Comput. Methods Appl. Mech. Engrg. 367 (2020) 113070.
[10] Qing Cheng, Jie Shen, Xiaofeng Yang, Highly efficient and accurate numerical schemes for the epitaxial thin film growth models by using the SAV approach, J. Sci. Comput. 78 (3) (2019) 1467–1487.
[11] Dong Li, Zhonghua Qiao, Tao Tang, Characterizing the stabilization size for semi-implicit fourier-spectral method to phase field equations, SIAM J. Numer. Anal. 54 (3) (2016) 1653–1681.
[12] Jie Shen, Jie Xu, Jiang Yang, The scalar auxiliary variable (SAV) approach for gradient flows, J. Comput. Phys. 353 (2018) 407–416.
[13] Xiaofeng Yang, Numerical approximations for the Cahn–Hilliard phase field model of the binary fluid-surfactant system, J. Sci. Comput. 74 (3) (2018) 1533–1553.
[14] S. Seirin Lee, S. Tashiro, A. Awazu, R. Kobayashi, A new application of the phase-field method for understanding the mechanisms of nuclear architecture reorganization, J. Math. Biol. 74 (1–2) (2017) 333–354.
[15] Fukeng Huang, Jie Shen, Zhiguo Yang, A highly efficient and accurate new scalar auxiliary variable approach for gradient flows, SIAM J. Sci. Comput. 42 (4) (2020) A2514–A2536.
[16] Zhengguang Liu, Xiaoli Li, The exponential scalar auxiliary variable (E-SAV) approach for phase field models and its explicit computing, SIAM J. Sci. Comput. 42 (3) (2020) B630–B655.
[17] Franck Boyer, Sebastian Minjeaud, Numerical schemes for a three component Cahn-Hilliard model, ESAIM Math. Model. Numer. Anal. 45 (4) (2011) 697–738.
[18] Xiaofeng Yang, Jia Zhao, Qi Wang, Jie Shen, Numerical approximations for a three-component Cahn–Hilliard phase-field model based on the invariant energy quadratization method, Math. Models Methods Appl. Sci. 27 (11) (2017) 1993–2030.
[19] Samuel M. Allen, John W. Cahn, A microscopic theory for antiphase boundary motion and its application to antiphase domain coarsening, Acta Metall. 27 (6) (1979) 1085–1095.
[20] John W. Cahn, John E. Hilliard, Free energy of a nonuniform system. I. Interfacial free energy, J. Chem. Phys. 28 (2) (1958) 258–267.
[21] John W. Cahn, John E. Hilliard, Free energy of a nonuniform system. III. Nucleation in a two-component incompressible fluid, J. Chem. Phys. 31 (3) (1959) 688–699.
[22] Steven M. Cox, Paul C. Matthews, Exponential time differencing for stiff systems, J. Comput. Phys. 176 (2) (2002) 430–455.
[23] J. Villain, Continuum models of crystal growth from atomic beams with and without desorption, J. Phys. I 1 (1) (1991) 19–42.
[24] Wenbin Chen, Cheng Wang, Xiaoming Wang, Steven M. Wise, A linear iteration algorithm for a second-order energy stable scheme for a thin film model without slope selection, J. Sci. Comput. 59 (3) (2014) 574–601.
[25] Edgar Avalos, Takeshi Higuchi, Takashi Teramoto, Hiroshi Yabu, Yasumasa Nishiura, Frustrated phases under three-dimensional confinement simulated by a set of coupled Cahn–Hilliard equations, Soft Matter 12 (27) (2016) 5905–5914.
[26] Edgar Avalos, Takashi Teramoto, Hideaki Komiyama, Hiroshi Yabu, Yasumasa Nishiura, Transformation of block copolymer nanoparticles from ellipsoids with striped lamellae into onionlike spheres and dynamical control via coupled Cahn–Hilliard Equations, ACS Omega 3 (1) (2018) 1304–1314.